Available online at www.sciencedirect.com
ScienceDirect
Journal of Solid State Chemistry 181 (2008) 415–422
JOURNAL OF SOLID STATE CHEMISTRY
www.elsevier.com/locate/jssc

Designing and tuning properties of a three-dimensional porous quaternary chalcogenide built on a bimetallic tetrahedral cluster $[M_4Sn_3S_{13}]^{5-}$ (M = Zn/Sn)

Min Wu[a], Thomas J. Emge[a], Xiaoying Huang[a], Jing Li[a,*], Yong Zhang[b]

[a]*Department of Chemistry and Chemical Biology Rutgers, The State University of New Jersey, Piscataway, NJ 08854, USA*
[b]*National Renewable Energy Laboratory, Golden, CO 80401, USA*

Received 14 November 2007; received in revised form 27 December 2007; accepted 30 December 2007
Available online 8 January 2008

Abstract

A multifunctional three-dimensional quaternary chalcogenide $[Na_5Zn_{3.5}Sn_{3.5}S_{13}]\cdot 6H_2O$ has been synthesized by solvothermal reactions. $[Na_5Zn_{3.5}Sn_{3.5}S_{13}]\cdot 6H_2O$ represents an interesting example of metal chalcogenides that combines semiconductivity, porosity, and light emission in a single structure. It crystallizes in the cubic space group Fm-3c, $a = 17.8630(3)$ Å, $V = 5699.85(17)$ Å^3, $Z = 8$. The compound decomposes at ~450 °C. A band gap of 2.9 eV is estimated from the optical diffuse reflectance data. A strong photoluminescence peak is observed at 2.43 eV in Mn doped samples. The electronic and optical properties of this compound can be systematically tuned by substitution of metal and chalcogen elements.

Keywords: Metal chalcogenide; Semiconductor; Open framework; Bimetallic cluster; Band gap; Photoluminescence; Multifunctionality

1. Introduction

Solid state metal chalcogenide materials have attracted considerable attention because of their superior semiconductor properties that can be used in numerous commercial applications, such as sensors, solar cells, solid electrolytes, and lasers [1–4]. Strong interests are generated recently in the design and synthesis of open-framework chalcogenides, in attempts of developing multifunctional materials that are capable of integrating porosity, electronic and optical properties in a single crystal structure and thus, hold promise for potential utility in areas such as catalysis, sorption, ion exchange, and gas storage, in addition to their useful optoelectronic properties. Design and understanding metal chalcogenide clusters can be very helpful for the development of porous chalcogenides, since many three-dimensional chalcogenides are constructed from these clusters. Some good examples of tetrahedral metal chalcogenide clusters have been reported for Groups 13–15 and transition metal elements [5].

A number of open-framework metal chalcogenides have been previously synthesized [5–8]. Most of these compounds are built upon regular supertetrahedral clusters Tn (Mt_nQt_{n+1}, M = metal, Q = S, Se, Te, $t_n = n(n+1)(n+2)/6$, $n \geqslant 1$) [6], or penta-supertetrahedral clusters Pn (($Mt_nQt_{n+1})_4$ (Qt_nMt_{n+1}) ($n \geqslant 1$)) [9]. These two common building units have the same geometrical features and follow the same construction rules. Single metal cations, or bimetallic cations in these supertetrahedral clusters are usually M^{2+}, M^{3+}, M^{4+}, [M^{4+}–M^{3+}] for T2, T3, and T4; [M^{+}–M^{3+}], [M^{2+}–M^{3+}] for T4, T5, and P2 ($M = Cu^+$, Zn^{2+}, Fe^{2+}, Co^{2+}, In^{3+}, Ga^{3+}, Sn^{4+}, Ge^{4+}, etc.) [9–14].

[M^{2+}–M^{4+}] chalcogenides are semiconductors containing a divalent (M^{2+}) transition metal chalcogenide and a tetravalent (M^{4+}) metal [15]. P1 (or partially distorted P1) and T3 cluster types for this combination have been reported [8,15–18]. While metal chalcogenides built upon supertetrahedral clusters have been investigated quite extensively, relatively little progress has been made on compounds made of other types of tetrahedral clusters.

*Corresponding author. Fax: +1 7324455312.
E-mail address: jingli@rci.rutgers.edu (J. Li).

0022-4596/$ - see front matter © 2008 Elsevier Inc. All rights reserved.
doi:10.1016/j.jssc.2007.12.035

Here we report an open-framework three-dimensional quaternary chalcogenide compound $[Na_5Zn_{3.5}Sn_{3.5}S_{13}]\cdot 6H_2O$ (**1**) that is constructed on a unique bimetallic tetrahedral cluster with systematically tunable properties.

2. Experimental section

2.1. Crystal growth and sample preparation

Single crystals of $[Na_5Zn_{3.5}Sn_{3.5}S_{13}]\cdot 6H_2O$ (**1**) were obtained in a reaction containing 0.50 mmol of Na_2S, 0.80 mmol of S, 0.25 mmol of Sn, and 0.017 mmol of $ZnCl_2$. The starting materials were pre-mixed and grinded, and then loaded in a 9 mm OD thick wall Pyrex tube. The sample was pre-heated at 90 °C for 1 h and followed by addition of 0.20 mL CH_3OH and 0.20 mL H_2O. The reaction was heated at 150 °C for 7 days. The products were washed with 80% alcohol followed by water. Pale yellow cubic crystals and crystalline powders with around 27% yield were obtained.

A series of experiments were carried out to substitute Zn metal by Mn and S by Se in compound **1**. The Mn and Se concentrations were varied between 3% and 20% based on Zn and S, respectively, employing the same synthesis route as used for **1**.

Table 1
Crystallographic data and structure refinement

Empirical formula	$Na_5Zn_{3.5}Sn_{3.5}S_{13}(H_2O)_6$
Formula weight	1284.04
Crystal size (mm)	$0.045 \times 0.043 \times 0.041$
Temperature (K)	100
Crystal system	Cubic
Space group	*Fm*-3*c* (No. 226)
Unit cell parameters (Å)	$a = 17.8630(3)$
V (Å^3)	5699.85(17)
Z	8
Calculated density (mg/m^3)	2.993
$F(000)$	4824
Absorption coefficient (mm^{-1})	6.961
λ (Å)	0.71073
θ range for data collection (deg)	2.28–30.50
Index ranges	$-25\leqslant h\leqslant 25$, $-25\leqslant k\leqslant 25$, $-25\leqslant l\leqslant 25$
Reflections collected	14,849
Independent reflections	738 [$R_{(int)} = 0.0516$]
Completeness to θ	100.0%
Refinement method	Full-matrix least-squares on F^2
Data/restraints/parameters	738/0/30
Goodness-of-fit on F^2	1.005
Final R indices [$I>2$sigma(I)]	$R_1 = 0.0261$, w$R_2 = 0.0583$
Absolute structure parameter	0.07(3)
R indices (all data)	$R_1 = 0.0278$, w$R_2 = 0.0595$
Largest diff. peak and hole (e/Å^3)	0.674 and −0.503

Table 2
Atomic coordinates ($\times 10^4$) and equivalent isotropic displacement parameters (Å$^2 \times 10^3$)

Atoms	x	y	z	U_{eq}
Sn(1)	0	5000	2500	11 (1)
M(2)[a]	764(1)	5764(1)	764(1)	11 (1)
Na(1)	3538(1)	6462(1)	1462(1)	26 (1)
S(1)	78(1)	6146(1)	1808(1)	8 (1)
S(2)	0	5000	0	14 (1)
Na(2)	2500	7500	2500	23 (1)
O(1)	3822(2)	7500	2500	18 (1)
H(1)	4040(40)	7840(40)	2240(40)	38 (19)

U_{eq} is defined as one-third of the trace of the orthogonalized U^{ij} tensor.
[a] $M = 0.125$Sn + 0.875Zn.

Table 3
Selected bond lengths (Å) and angles (deg)

Sn(1)–S(1)	2.3951(9)	Na(1)–S(1)#10	2.875(2)
Sn(1)–S(1)#1	2.3952(9)	S(1)–Na(1)#11	2.875(2)
Sn(1)–S(1)#2	2.3952(9)	S(2)–M(2)#12	2.3648(8)
Sn(1)–S(1)#3	2.3952(9)	S(2)–M(2)#1	2.3648(8)
M(2)–S(1)#4	2.3331(9)	S(2)–M(2)#13	2.3648(8)
M(2)–S(1)#5	2.3331(9)	Na(2)–O(1)	2.361(4)
M(2)–S(1)	2.3331(9)	Na(2)–O(1)#6	2.362(4)
M(2)–S(2)	2.3647(8)	Na(2)–O(1)#4	2.362(4)
Na(1)–O(1)	2.671(3)	Na(2)–O(1)#7	2.362(4)
Na(1)–O(1)#6	2.671(3)	Na(2)–O(1)#5	2.362(4)
Na(1)–O(1)#7	2.671(3)	Na(2)–O(1)#14	2.362(4)
Na(1)–S(1)#8	2.875(2)	O(1)–Na(1)#15	2.671(3)
Na(1)–S(1)#9	2.875(2)	O(1)–H(1)	0.86(7)
S(1)–Sn(1)–S(1)#1	117.86(4)	M(2)–S(1)–Sn(1)	101.15(3)
S(1)–Sn(1)–S(1)#2	105.45(2)	M(2)–S(1)–Na(1)#11	112.83(7)
S(1)#1–Sn(1)–S(1)#2	105.45(2)	Sn(1)–S(1)–Na(1)#11	102.89(3)
S(1)–Sn(1)–S(1)#3	105.45(2)	M(2)–S(2)–M(2)#12	109.5
S(1)#1–Sn(1)–S(1)#3	105.45(2)	M(2)–S(2)–M(2)#1	109.5
S(1)#2–Sn(1)–S(1)#3	117.86(4)	M(2)#12–S(2)–M(2)#1	109.5
S(1)#4–M(2)–S(1)#5	109.87(3)	M(2)–S(2)–M(2)#13	109.5
S(1)#4–M(2)–S(1)	109.87(3)	M(2)#12–S(2)–M(2)#13	109.5
S(1)#5–M(2)–S(1)	109.87(3)	M(2)#1–S(2)–M(2)#13	109.5
S(1)#4–M(2)–S(2)	109.07(3)	O(1)–Na(2)–O(1)#6	90.0
S(1)#5–M(2)–S(2)	109.07(3)	O(1)–Na(2)–O(1)#4	90.0
S(1)–M(2)–S(2)	109.07(3)	O(1)#6–Na(2)–O(1)#4	180.0
O(1)–Na(1)–O(1)#6	77.37(17)	O(1)–Na(2)–O(1)#7	90.0
O(1)–Na(1)–O(1)#7	77.37(17)	O(1)#6–Na(2)–O(1)#7	90.0
O(1)#6–Na(1)–O(1)#7	77.37(17)	O(1)#4–Na(2)–O(1)#7	90.0
O(1)–Na(1)–S(1)#8	78.78(9)	O(1)–Na(2)–O(1)#5	90.000(1)
O(1)#6–Na(1)–S(1)#8	118.53(4)	O(1)#6–Na(2)–O(1)#5	90.0
O(1)#7–Na(1)–S(1)#8	147.27(5)	O(1)#4–Na(2)–O(1)#5	90.0
O(1)–Na(1)–S(1)#9	118.53(4)	O(1)#7–Na(2)–O(1)#5	180.0
O(1)#6–Na(1)–S(1)#9	147.27(5)	O(1)–Na(2)–O(1)#14	180.0
O(1)#7–Na(1)–S(1)#9	78.78(9)	O(1)#6–Na(2)–O(1)#14	90.000(1)
S(1)#8–Na(1)–S(1)#9	93.46(10)	O(1)#4–Na(2)–O(1)#14	90.0
O(1)–Na(1)–S(1)#10	147.27(5)	O(1)#7–Na(2)–O(1)#14	90.000(1)
O(1)#6–Na(1)–S(1)#10	78.78(9)	O(1)#5–Na(2)–O(1)#14	90.0
O(1)#7–Na(1)–S(1)#10	118.53(4)	Na(2)–O(1)–H(1)	117(5)
S(1)#8–Na(1)–S(1)#10	93.46(10)	Na(1)#15–O(1)–H(1)	88(5)
S(1)#9–Na(1)–S(1)#10	93.46(10)	Na(1)–O(1)–H(1)	102(5)

Symmetry transformations used to generate equivalent atoms: #1, $-x,-y+1,z$; #2, $y-1/2,-x+1/2,-z+1/2$; #3, $-y+1/2$, $x+1/2$, $-z+1/2$; #4, $y-1/2$, $z+1/2$, x; #5, $z,x+1/2,y-1/2$; #6, $-y+1,z+1/2,-x+1/2$; #7, $z,-x+1,-y+1$; #8, $x+1/2,z+1/2,y-1/2$; #9, $-y+1,-x+1/2$, $z+0$; #10, $-z+1/2,y+0,-x+0$; #11, $-y+1/2,-x+1,z+0$; #12, $x,-y+1,-z$; #13, $-x,y,-z$; #14, $-x+1/2,-y+3/2$, z; #15, $x,-y+3/2,-z+1/2$; #16, $-x+1/2,y,-z+1/2$.

2.2. Structure characterization, optical absorption and thermal analysis

Single crystal X-ray diffraction of **1** was carried out on a Bruker-AXS smart APEX CCD diffractometer with graphite-monochromated Mo$K\alpha$ radiation ($\lambda = 0.71073$ Å). All calculations were performed using the SHELXL-97 crystallographic software package. The data were collected at a temperature 100(2) K to a maximum θ value of 30.50°. Of a total of 14,849 reflections collected, 738 were independent ($R_{int} = 0.0516$). The structure was solved by direct methods and expanded using Fourier techniques. The non-hydrogen atoms were refined anisotropically and the hydrogen atom was refined isotropically. The final cycle of full matrix least-squares refinement on F^2 was based on 716 observed reflections as well as 30 variable parameters and converged at $R_1 = 0.0261$. The unit cell parameters, along with data collection and refinement details, are listed in Table 1. Atomic coordinates and equivalent isotropic temperature factors are listed in Table 2. Shown in Table 3 are selected bond lengths (Å) and bond angles (°).

The phase purity of all samples was analyzed by powder X-ray diffraction using a Rigaku D/M-2200T automated diffraction system (Ultima+). The measurements were made with a 2θ range between 3° and 70° at the operation power of 40 kV/40 mA. The band gaps of **1** and all substituted samples were assessed by optical diffuse reflectance experiments at room temperature. All measurements were made on a Shimadzu UV-3101PC double beam, double monochromated spectrophotometer in the range of 250–2000 nm. Thermogravimetric analysis (TGA) was carried out on a TA Instrument Q50 Thermogravimetric analyzer with a ramp rate of 15 °C/min from room temperature to 700 °C under nitrogen. Differential scanning calorimetry (DSC) experiments were performed on a TA Instrument Q100 from room temperature to 500 °C with a ramp rate of 10 °C/min.

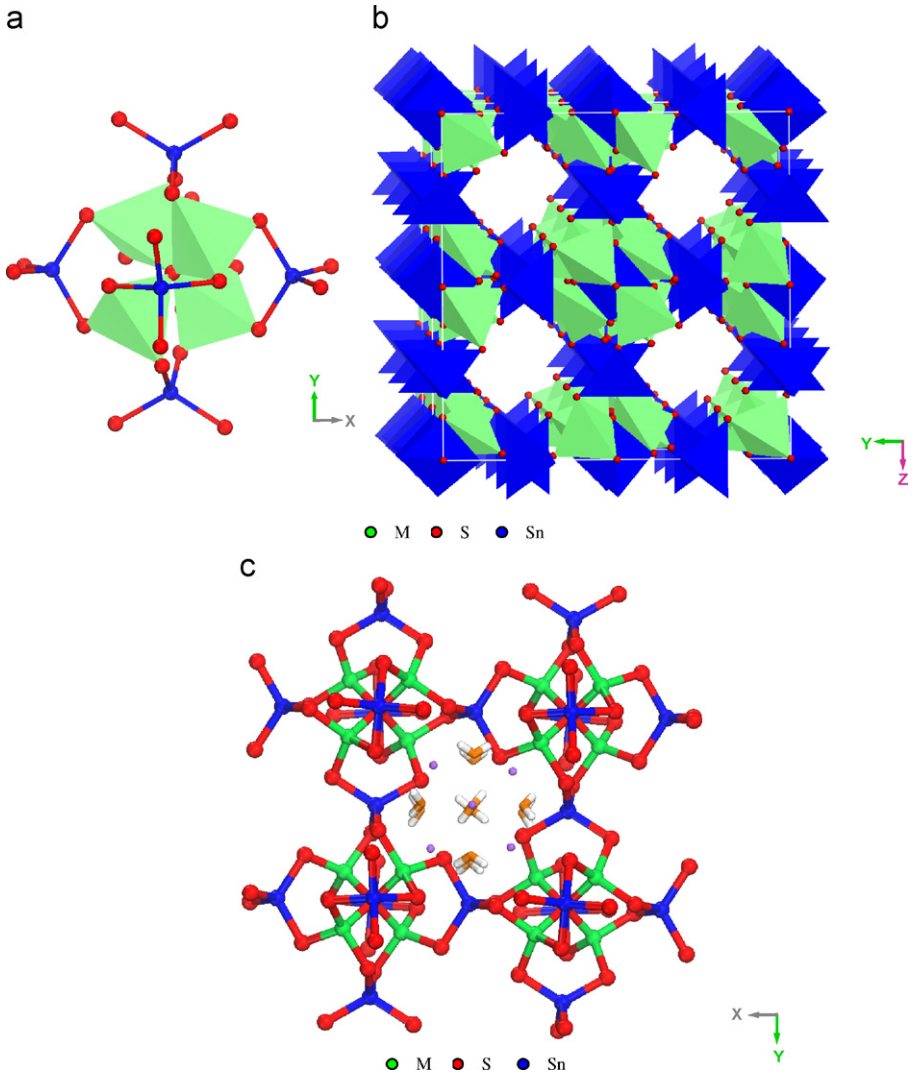

Fig. 1. (a) SM_4(SnS_4)$_6$ cluster (M = Zn, Sn). (b) View of the three-dimensional network without Na cations and H_2O molecules. (c) Highly symmetric pore with Na cations (purple) and H_2O molecules.

2.3. Photoluminescence spectroscopy

Photoluminescence (PL) was measured at room temperature with a SPEX 1403 spectrometer, RCAC31034 GaAs PMT, and the 325 nm line of a He–Cd laser with ~5 mW power.

2.4. Solvent exchange experiments

In order to evaluate the exchange capability of the solvent molecules in the pores, experiments were carried out to exchange water with dimethyl sulfoxide(DMSO). The samples were heated by TGA to remove all water molecules inside the pores while keeping the framework structure intact. After TGA, the samples were analyzed by powder X-ray diffraction and followed by addition of water and DMSO, respectively. The samples were placed in these solvents and heated at ~60 °C for a few hours and then left at room temperature for 2 days. The final products were washed with ethyl ether several times and dried in the air. PXRD and TGA were carried out again with the same procedure as before.

3. Results and discussion

The building block of the three-dimensional $[Na_5Zn_{3.5}Sn_{3.5}S_{13}]\cdot 6H_2O$ (**1**) structure is a bimetallic cluster $[M_4Sn_3S_{13}]^{5-}$, which consists of four MS_4 ($M = 0.125Sn + 0.875Zn$) tetrahedra that share a corner of S atom at the core, and $6 \times \frac{1}{2}$ terminal SnS_4 tetrahedra. Two of the S atoms in each SnS_4 tetrahedron are corner-shared with two MS_4 tetrahedra within the same cluster while the other two S atoms link to two MS_4 tetrahedra in the adjacent cluster by corner-sharing. The building block can also be conveniently written as $[(SM_4)(SnS_4)_{6/2}]$ or $[M_4Sn_3S_{13}]^{5-}$, since its core can be considered as an SM_4 tetrahedron [19], and since each of the six outer SnS_4 tetrahedra is shared with an adjacent cluster (Fig. 1a). Each cluster is linked to six adjacent clusters through S–S edge of SnS_4 tetrahedra in *a*, *b*, *c* directions, respectively, to form a three-dimensional network structure. The three-dimensional network of **1** contains open channels running through all three directions (Fig. 1b). The smallest cross section of the channels measured approximately 5.4×5.4 Å (between the centers of sulfur atoms). There are two crystallographic independent Na atoms. Each of the four Na(1) atoms are located at the corner of channels surrounded by three H_2O molecules in the channel and three S atoms from the framework. The Na(2) atom is found in the center of the channel with six surrounding H_2O molecules forming an octahedron. The pore volume (when excluding Na^+ and H_2O) was calculated to be 1613.9 $Å^3$ using the SOLV routine in PLATON [20], around 28.3% of the volume within a unit cell.

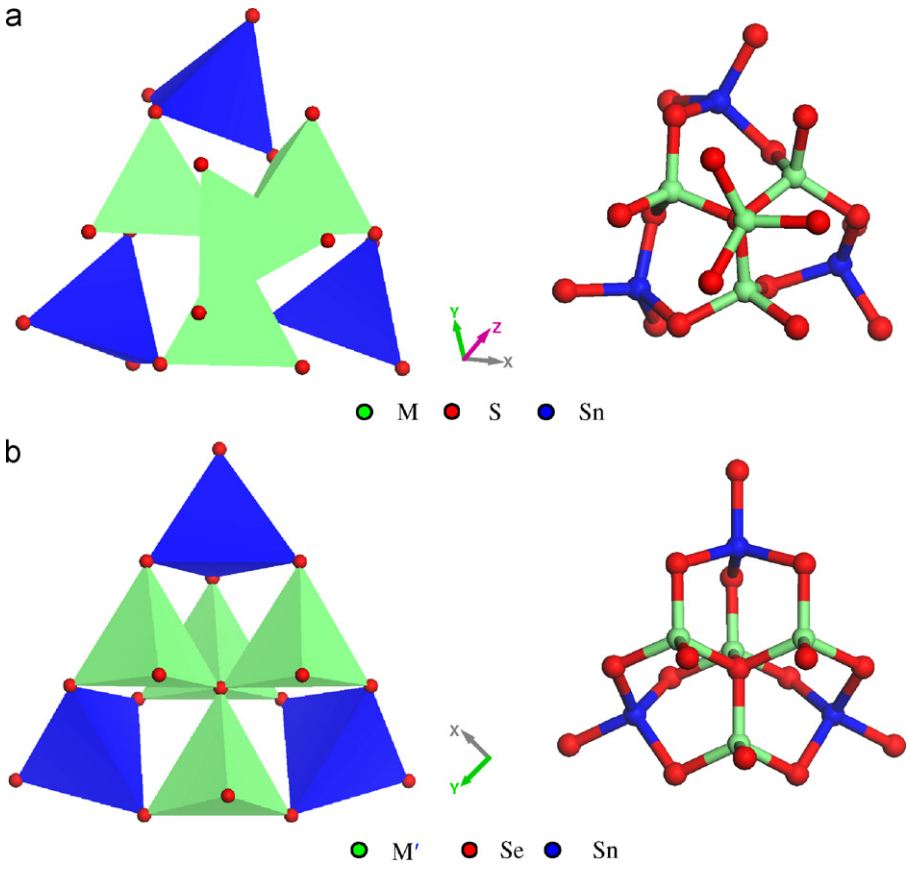

Fig. 2. (a) Building block of $[M_4Sn_3S_{13}]^{5-}$ ($M = 0.125Sn + 0.875Zn$) in **1**; (b) building block of $[M_4'Sn_3Se_{13}]^{6-}$ ($M' = Zn$, Hg) in $K_3Rb_3Zn_4Sn_3Se_{13}$ and $K_6Hg_4Sn_3Se_{13}\cdot MeOH(H_2O)_3$.

Fig. 2 shows the similarities and differences of the $[M_4Sn_3S_{13}]^{5-}$ ($M = 0.125Sn + 0.875Zn$) building unit in **1** in comparison with $[M_4'Sn_3Se_{13}]^{6-}$ ($M' = Zn$ [21], Hg [14]) in $K_3Rb_3Zn_4Sn_3Se_{13}$ and $K_6Hg_4Sn_3Se_{13} \cdot MeOH(H_2O)_3$. There are two crystallographically independent Zn/Hg sites for the four inner $ZnSe_4$ or $HgSe_4$ tetrahedra, while the four inner MS_4 tetrahedra in the $[M_4Sn_3S_{13}]^{5-}$ cluster are identical. The $[M_4Sn_3S_{13}]^{5-}$ cluster possess higher symmetry T_d, while the symmetry is a lower C_{3v} for $[Zn_4Sn_3Se_{13}]^{6-}$ and $[Hg_4Sn_3Se_{13}]^{6-}$ clusters. Each of the three surrounding $SnSe_4$ tetrahedra in $[Zn_4Sn_3Se_{13}]^{6-}$corner shares Se of three $ZnSe_4$ tetrahedra in the core, leaving one Se atom corner-shared by another $ZnSe_4$ tetrahedron from the adjacent cluster, while in $[M_4Sn_3S_{13}]^{5-}$ each of the three surrounding SnS_4 tetrahedra corner shares S of two MS_4 tetrahedra in the core, leaving two S atoms corner-shared by another MS_4 tetrahedron from the adjacent cluster.

This light yellow material of **1** is stable in air and water. The thermal stability was studied via TGA conducted on pure polycrystalline samples. Fig. 3a shows the TG profile for the temperature range between room temperature and 700 °C. The sample began to lose water molecule at ~150 °C and completed the process at ~350 °C with a total loss of 8.1%, in reasonable agreement with the calculated value of 8.4%. The compound decomposed around 450 °C. The high thermal stability may be due to high framework symmetry and the higher charged Sn^{4+} metal sites which provide sufficient bond valences to balance the edge or corner S^{2-} anions [22]. DSC profile in Fig. 3b shows two endothermic peaks at ~180 °C (small) and 350 °C (large), both correspond to the release of water molecules. The exothermic peak at ~440–450 °C is due to the decomposition, producing several binary phases (ZnS, ZnO, SnO_2). Powder X-ray diffraction was performed immediately after heating up to 350 °C for 1 h. Clearly there are some minor changes in the X-ray pattern, but major peaks are retained, indicating that the framework structure of the material is preserved.

One way to tune the electronic and optical properties of materials is by alloying or doping/substitution. We investigated substitution effect by replacing Zn with Mn and S with Se. No phase separation was observed in the concentration range of 3–20% based on the powder X-ray analysis. The PXRD patterns of the substituted samples are shown in Fig. 4. The optical properties were studied by measuring the room temperature diffuse reflectance of **1** as well as Mn and Se substituted samples. The optical spectra of **1**, along with Mn and Se substituted samples are plotted in Fig. 5a and b, respectively. The sharp absorption edge was observed at ~2.9 eV for **1**. As the concentration of Se and Mn was increased, a red shift in the band gap was achieved, as expected based on the atomic properties of the substituents. The shoulder around ~2 eV in the optical spectra of the Mn doped materials may be due to mid-gap states associated with Mn^{2+} *d–d* transitions. For Se doped samples, the band gap varies smoothly and can be well defined as in II–VI semiconductor alloys involving S and

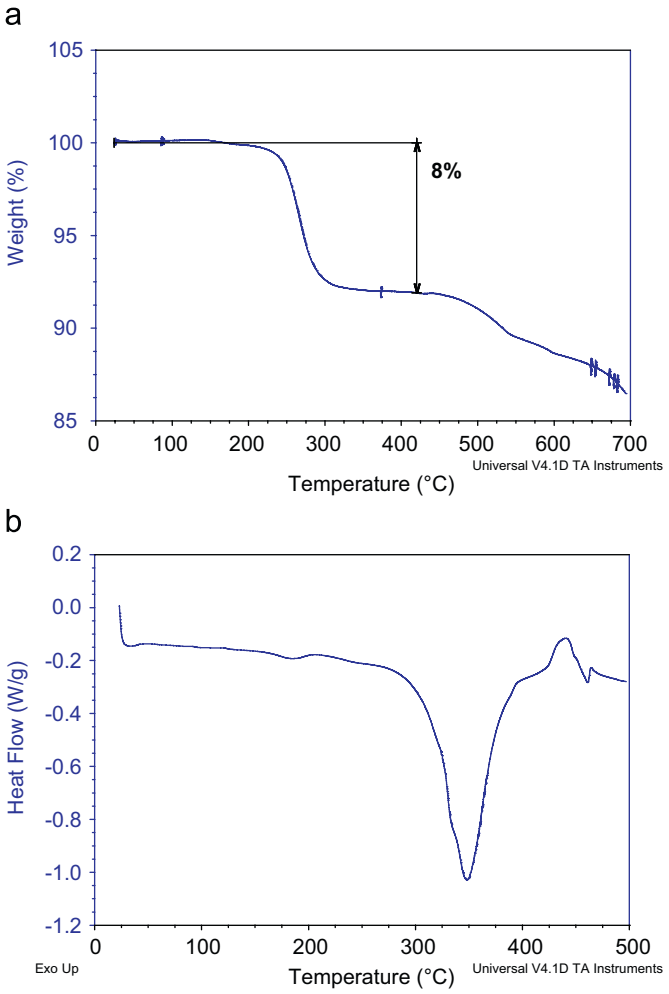

Fig. 3. (a) TG profile and (b) DSC plot for compound **1**.

Se. Fig. 6 shows a nice linear relationship of the band gap energy as a function of Se concentration. However, for the Mn doped samples, because Mn is strongly mismatched with the host element Zn, on one hand, the doping leads to the red shift of the host band gap; on the other hand, it generates an impurity state below the band gap which eventually evolves into a new absorption band (a small lump at around 2.0 eV) that merges with the perturbed host absorption band. The effect of Mn doping is at least to some extent similar to that in other systems of isoelectronic doping [23].

Fig. 7 shows the TGA results before and after solvent exchange with DMSO. Fig. 7a indicated all water molecules inside the channels were removed with a weight loss around 7.9% (above 100 °C). The weight loss below 100 °C was primarily from the solvents on the surface. Another TG was carried out on the sample after being immersed in DMSO, and removed the excess DMSO on the surface by washing with ethyl ether several times. The second TGA (Fig. 7b) gave ~4.94% weight loss from 100 °C, which indicates approximately one DMSO molecule replaced six H_2O molecules inside the pores. Powder

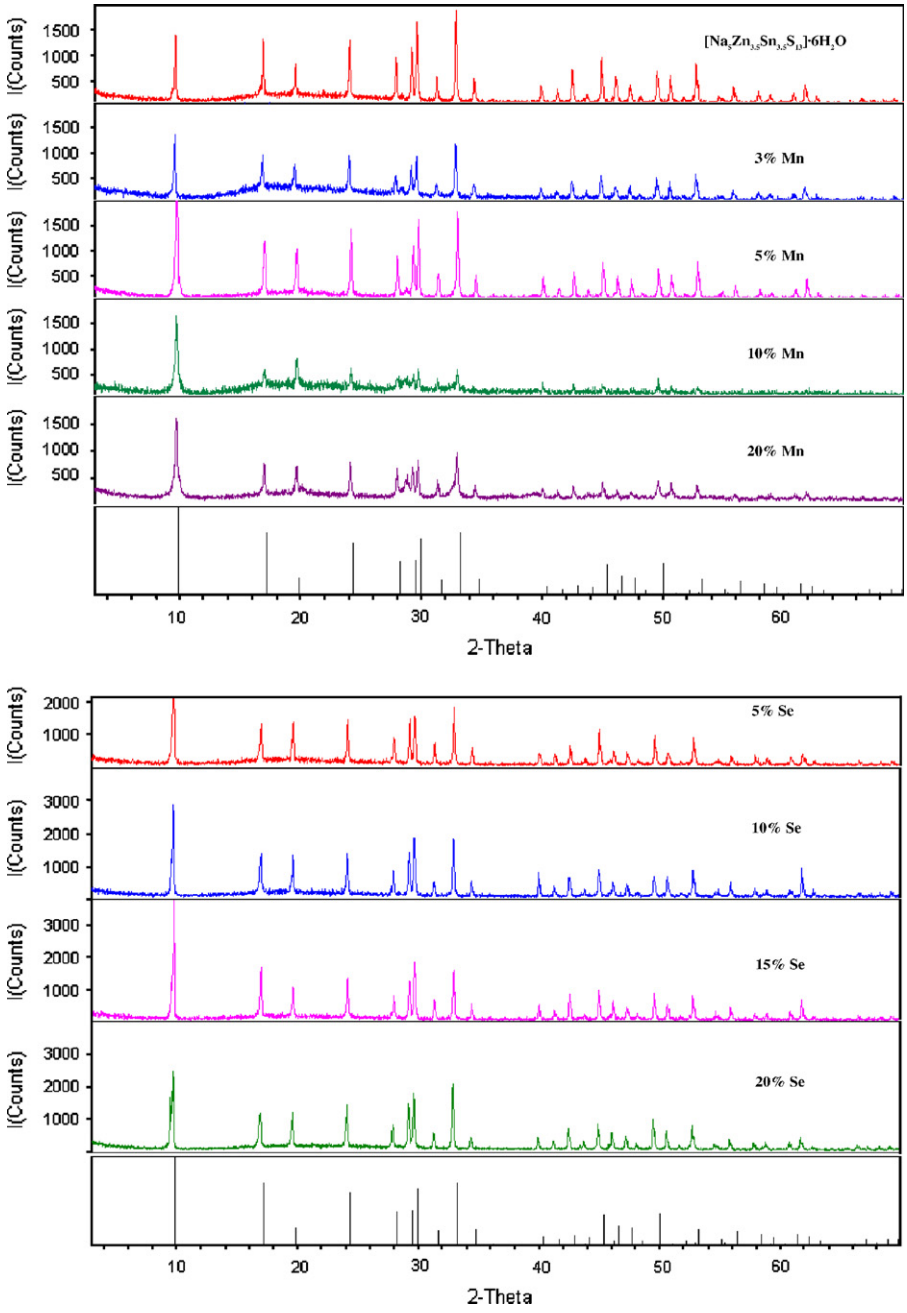

Fig. 4. Powder X-ray diffraction patterns of $[Na_5Zn_{3.5}Sn_{3.5}S_{13}]\cdot 6H_2O$ and Mn, Se substituted compounds with the substituent concentration between 3% and 20%. (black lines: simulated pattern from the single crystal data).

X-ray diffraction showed the structure remained the same before and after TGA. Water restoration experiment was performed as well with the same procedure. It gave around 4% weight loss from 100 °C, indicating the H_2O molecules can reenter the open channels fairly easily.

Fig. 8 shows the PL spectra of **1** with Mn concentration varying from 0% to 20%, measured at room temperature. The powder was held in a quartz vial. The emission of 0% sample is very weak. With increasing Mn concentration, a PL band at 2.03–2.04 eV appears and its intensity increases continuously. The peak energy is consistent with that of Mn content in II–VI semiconductors, and the energy is insensitive to the host [24]. The emission above the Mn related band seems to also enhance with increasing Mn doping level. The origin is unclear, but could be defect related, which deserves further investigation.

4. Concluding remarks

In summary, a new open-framework quaternary metal chalcogenide compound $[Na_5Zn_{3.5}Sn_{3.5}S_{13}]\cdot 6H_2O$ built on an bimetallic tetrahedral cluster $[M_4Sn_3S_{13}]^{5-}$ ($M = 0.125Sn + 0.875Zn$), has been synthesized and characterized. The compound combines semiconductor properties

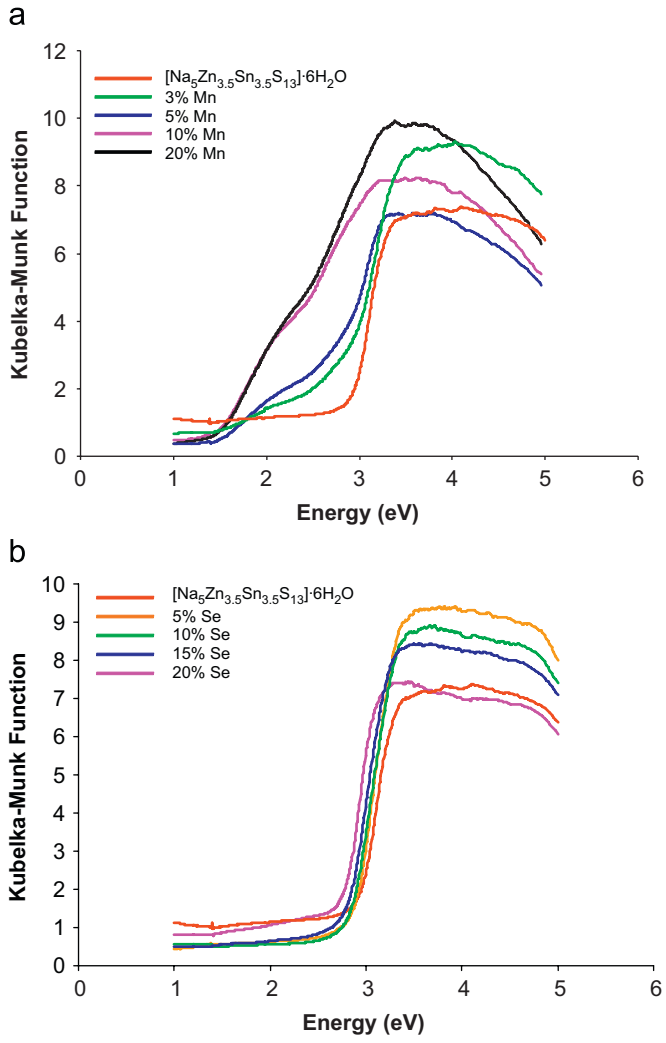

Fig. 5. (a) Optical absorption spectra of **1** and 3%, 5%, 10%, and 20% Mn substituted compounds. (b) Optical absorption spectra of **1** and 5%, 10%, 15%, and 20% Se substituted compounds.

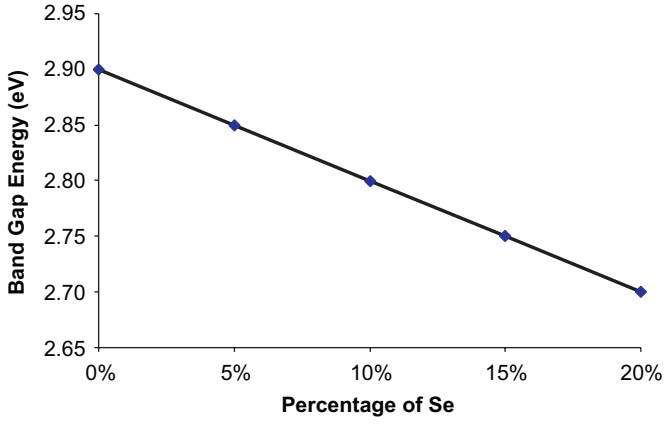

Fig. 6. Band gap energy as a function of Se concentration in **1**.

with other interesting functionality such as porosity in a single structure. The successful doping/substitution of Mn and Se allows systematic tuning of the band gap and optical properties of this semiconductor compound. The

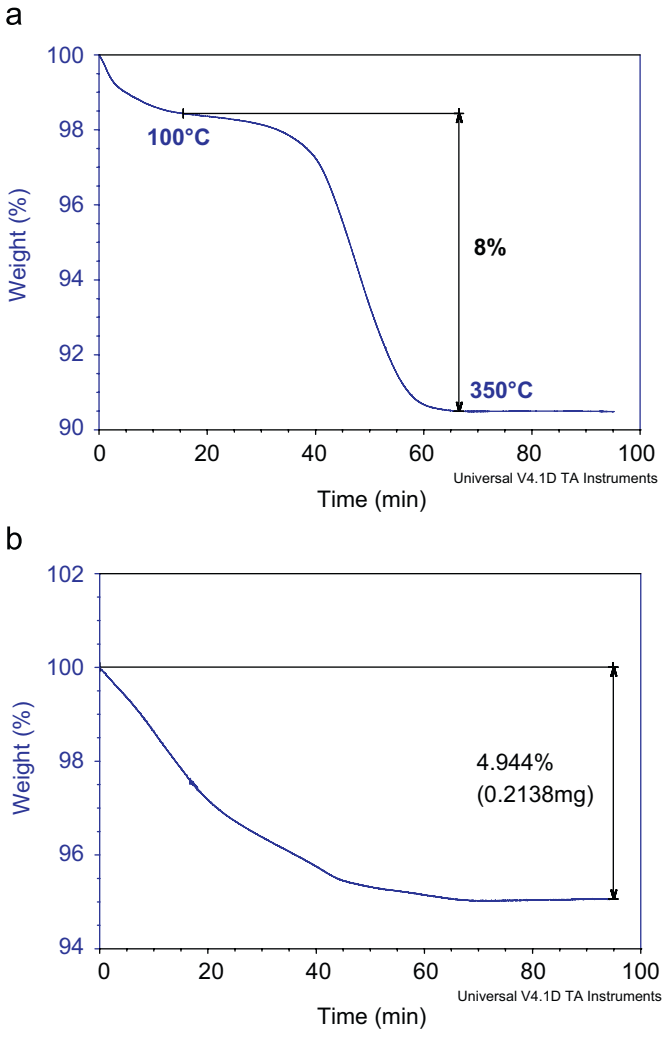

Fig. 7. (a) TG profile showing removal of water molecules in the channels. (b) TG profile after the exchange by DMSO. A weight loss of 4.94% was observed.

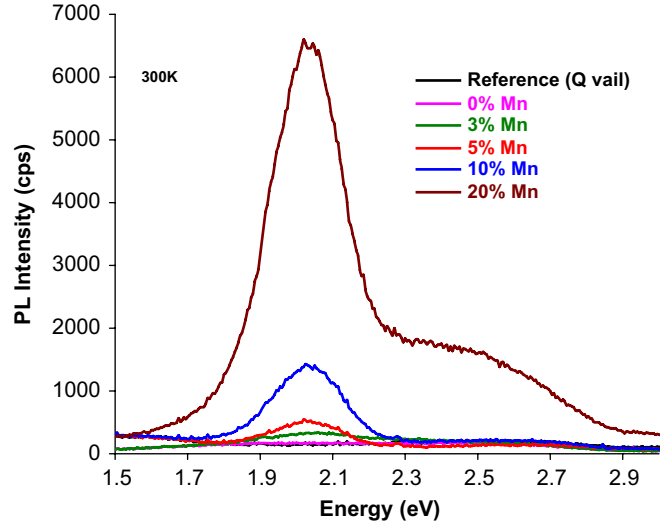

Fig. 8. Room temperature photoluminescence of Mn doped $[Na_5Zn_{3.5}Sn_{3.5}S_{13}]\cdot 6H_2O$ with varying Mn concentration.

relatively large band gap (~3 eV) makes it a promising candidate as a transparent conducting material, if either n- or p-type doping should be shown feasible. Since it is a non-oxide large band gap material, it is of particular interest for the application as a p-type transparent conducting material. The study of solvent exchange indicates that the guest molecules in the open pores can be easily taken out and restored without changing the framework structure. This work provides useful information for the future design and synthesis of new metal chalcogenides with desired multifunctionality.

Acknowledgments

We are grateful to the National Science Foundation for the generous support of this research through Grant DMR-0422932. Work at NREL was supported by NREL LDRD (#06590504).

References

[1] T. Ohta, K. Nishiuchi, K. Narumi, Y. Kitaoka, H. Ishibashi, N. Yamada, T. Kozaki, Jpn. J. Appl. Phys. Part 1—Regular Papers Short Notes & Review Papers 39 (2000) 770–774.
[2] T. Akiyama, K. Yoshioka, K. Inoue, H. Isomura, T. Ohta, Opt. Rev. 2 (1995) 100–102.
[3] S. Dhingta, M.G. Kanatzidis, Science 258 (1992) 1769.
[4] A. Shah, P. Torres, R. Tscharner, N. Wyrsch, H. Keppner, Science 285 (1999) 692–698.
[5] X.H. Bu, N.F. Zheng, P.Y. Feng, Chemistry—a Eur. J. 10 (2004) 3356–3362.
[6] H.L. Li, A. Laine, M. O'Keeffe, O.M. Yaghi, Science 283 (1999) 1145–1147.
[7] H.L. Li, J. Kim, T.L. Groy, M. O'Keeffe, O.M. Yaghi, J. Am. Chem. Soc. 123 (2001) 4867–4868.
[8] N. Ding, D.Y. Chung, M.G. Kanatzidis, Chem. Commun. (2004) 1170–1171.
[9] N.F. Zheng, X.H. Bu, P.Y. Feng, Angew. Chem.—Int. Ed. 43 (2004) 4753–4755.
[10] X.H. Bu, N.F. Zheng, Y.Q. Li, P.Y. Feng, J. Am. Chem. Soc. 124 (2002) 12646–12647.
[11] N.F. Zheng, X.G. Bu, B. Wang, P.Y. Feng, Science 298 (2002) 2366–2369.
[12] C. Wang, Y.Q. Li, X.H. Bu, N.F. Zheng, O. Zivkovic, C.S. Yang, P.Y. Feng, J. Am. Chem. Soc. 123 (2001) 11506–11507.
[13] C.L. Cahill, J.B. Parise, J. Chem. Soc.—Dalton Trans. 9 (2000) 1475–1482.
[14] C.L. Cahill, J.B. Parise, Chem. Mater. 9 (1997) 807–811.
[15] M.K. Brandmayer, R. Clerac, F. Weigend, S. Dehnen, Chem.—Eur. J. 10 (2004) 5147–5157.
[16] M. Wu, J. Li, X.Y. Huang, W.P. Su, Abstr. Pap. Am. Chem. Soc. 228 (2004), U813–U813.
[17] M.J. Manos, R.G. Iyer, E. Quarez, J.H. Liao, M.G. Kanatzidis, Angew. Chem.—Int. Ed. 44 (2005) 3552–3555.
[18] C. Zimmermann, C.E. Anson, F. Weigend, R. Clerac, S. Dehnen, Inorg. Chem. 44 (2005) 5686–5695.
[19] N.F. Zheng, X.H. Bu, P.Y. Feng, J. Am. Chem. Soc. 127 (2005) 5286–5287.
[20] A.L. Spek, PLATON, a multipurpose crystallographic tool, Utrecht, 2005.
[21] M. Wu, W.P. Sul, N. Jasutkar, X.Y. Huang, J. Li, Mater. Res. Bull. 40 (2005) 21–27.
[22] P.Y. Feng, X.H. Bu, N.F. Zheng, Acc. Chem. Res. 38 (2005) 293–303.
[23] Y. Zhang, B. Fluegel, A. Mascarenhas, H.P. Xin, C.W. Tu, Phys. Rev. B 62 (2000) 4493–4500.
[24] B. Tripathi, Y.K. Vijay, S. Wate, F. Singh, D.K. Avasthi, Solid-State Electron. 51 (2007) 81–84.